

# UC Berkeley

## UC Berkeley Previously Published Works

### Title

Ciliary localization of a light-activated neuronal GPCR shapes behavior.

### Permalink

<https://escholarship.org/uc/item/2c99q9vw>

### Journal

Proceedings of the National Academy of Sciences, 120(43)

### Authors

Winans, Amy

Friedmann, Drew

Stanley, Cherise

et al.

### Publication Date

2023-10-24



### DOI

10.1073/pnas.2311131120

Peer reviewed



# Ciliary localization of a light-activated neuronal GPCR shapes behavior

Amy M. Winans<sup>a</sup>, Drew Friedmann<sup>a,1</sup>, Cherise Stanley<sup>a</sup>, Tong Xiao<sup>b</sup>, Tsung-li Liu<sup>c,2</sup>, Christopher J. Chang<sup>a,b,d</sup> , and Ehud Y. Isacoff<sup>a,d,e,f,3</sup> 

Contributed by Ehud Y. Isacoff; received July 3, 2023; accepted September 12, 2023; reviewed by Angeles B. Ribera and Mark Van Zastrow

Many neurons in the central nervous system produce a single primary cilium that serves as a specialized signaling organelle. Several neuromodulatory G-protein-coupled receptors (GPCRs) localize to primary cilia in neurons, although it is not understood how GPCR signaling from the cilium impacts circuit function and behavior. We find that the vertebrate ancient long opsin A (VALopA), a G<sub>i</sub>-coupled GPCR extraretinal opsin, targets to cilia of zebrafish spinal neurons. In the developing 1-d-old zebrafish, brief light activation of VALopA in neurons of the central pattern generator circuit for locomotion leads to sustained inhibition of coiling, the earliest form of locomotion. We find that a related extraretinal opsin, VALopB, is also G<sub>i</sub>-coupled, but is not targeted to cilia. Light-induced activation of VALopB also suppresses coiling, but with faster kinetics. We identify the ciliary targeting domains of VALopA. Retargeting of both opsins shows that the locomotory response is prolonged and amplified when signaling occurs in the cilium. We propose that ciliary localization provides a mechanism for enhancing GPCR signaling in central neurons.

opsin | cilium | zebrafish | VALopA | central pattern generator

Primary cilia are microtubule-based “signaling hubs” that protrude from many cell types, including most neurons. Mutations that perturb ciliary function are associated with a range of disorders, termed “ciliopathies,” which affect a wide array of physiological systems, including the nervous system (1). Intricate gate-keeping systems control the influx and efflux of components between the cell body and ciliary membrane and cilioplasm, allowing for enrichment of some signaling systems (2). More than two dozen G-protein-coupled receptors (GPCRs) have been identified as enriched in the ciliary membrane (3). GPCR signaling through primary cilia in neural systems has been shown to be critical for development through Hedgehog, Wnt, and other signaling pathways (4), as recently illustrated by Truong et al. who showed that cyclic adenosine monophosphate (cAMP) in the cilium, but not in the cell body, regulates Hedgehog-dependent development in zebrafish (5). Recent studies have also pointed to an important role for ciliary GPCR signaling in neural transmission and downstream behavior.

Many neuromodulatory GPCRs localize to primary cilia in the brain [e.g., dopamine receptors 1 and 5, serotonin receptor 6, somatostatin receptor 3 (SSTR3), and others] (3). Inhibition of adenylyl cyclase signaling in primary cilia in the hypothalamus leads to increased feeding and obesity, likely through the melanocortin system (6). Knocking out or inhibiting ciliary-localized SSTR3 impairs object recognition memory (7). Recently, Sheu et al. demonstrated that axons can synapse onto primary cilia, activate ciliary serotonin receptors, and modulate chromatin accessibility (8). However, it remains unclear why specific GPCR subtypes are localized to cilia and how signaling in the cell body versus primary cilium differ in the regulation of neuronal cell and circuit function and behavior.

To probe how ciliary localization of GPCRs may modulate behavior, we aimed to compare how the activation of a GPCR in the primary cilium versus a GPCR in the cell body differed in its effect on downstream behavior. We previously showed that blue-green light activation of a vertebrate ancient long opsin A (VALopA), an extraretinal, G<sub>i</sub>-coupled opsin GPCR that is expressed in the embryonic zebrafish spinal cord (9–11), inhibits the early precursor to swimming, coiling, in the 1 d post fertilization (1 dpf) fish. Coiling is driven by the central pattern generator (CPG) circuit in the spinal cord and develops rapidly into the coordinated side-to-side alternating rhythm that controls swim behavior (12, 13). Here, we find that VALopA localizes to cilia. Remarkably, VALopB, a homologous [67% amino acid (AA) identity] blue-green opsin, which is found outside of the spinal cord in the embryonic zebrafish (11), localizes to the cell body. VALopB is also G<sub>i</sub>-coupled and photo-inhibits coiling when expressed in the spinal cord CPG circuit, but with different dynamics.

## Significance

VALopA is an extraretinal opsin G-protein-coupled receptor that is expressed in the locomotory central pattern generator (CPG) neurons of the developing spinal circuit of zebrafish. VALopA provides direct sensory input to modulate motor circuit output, whereby brief pulses of light induce a profound and long-lasting inhibition of early locomotor behavior. We find that VALopA is localized to the primary cilia of CPG neurons. A related extraretinal opsin, VALopB, which, like VALopA, is G<sub>i</sub>-coupled, is not targeted to cilia. We map the ciliary targeting signals and find that retargeting into cilia has two striking effects: prolongation and amplification of the inhibitory light response. We propose that ciliary localization provides a general mechanism for enhancing GPCR signaling in central neurons.

Author contributions: A.M.W., D.F., T.X., and E.Y.I. designed research; A.M.W., D.F., T.X., and E.Y.I. performed research; A.M.W., D.F., C.S., and T.X. contributed new reagents/analytic tools; A.M.W., D.F., T.X., T.-I.L., C.J.C., and E.Y.I. analyzed data; T.-I.L. supported microscopy; C.J.C. oversaw research; and A.M.W. and E.Y.I. wrote the paper.

Reviewers: A.B.R., University of Colorado; and M.V.Z., University of California San Francisco.

The authors declare no competing interest.

Copyright © 2023 the Author(s). Published by PNAS. This article is distributed under [Creative Commons Attribution-NonCommercial-NoDerivatives License 4.0 \(CC BY-NC-ND\)](https://creativecommons.org/licenses/by-nc-nd/4.0/).

<sup>1</sup>Present address: Cajal Neuroscience Inc., High-throughput Imaging, Seattle, WA 98102.

<sup>2</sup>Present address: Qureator Inc., Engineering, San Diego, CA 92121.

<sup>3</sup>To whom correspondence may be addressed. Email: ehud@berkeley.edu.

This article contains supporting information online at <https://www.pnas.org/lookup/suppl/doi:10.1073/pnas.2311131120/-/DCSupplemental>.

Published October 16, 2023.

We identify the targeting motifs that localize VALopA to cilia and use these, as well as fusion to other cilia-targeted proteins, to assess the functional impact of ciliary targeting. We find that ciliary localization of opsins increases the locomotory response to light, suggesting that it provides a mechanism for signal amplification and prolongation.

## Results

**VALopA Localizes to Primary Cilia.** The 1020:Gal4 zebrafish line drives expression in neurons of the locomotory CPG and in Kolmer–Agduhr (KA) cells, also known as CSF-contacting neurons, in embryonic and larval zebrafish (12, 14, 15). Previously, RNAseq analysis revealed that pooled 1020:Gal4 neurons express VALopA, which mediates blue-green light-triggered inhibition of coiling, the early locomotory behavior that takes place as CPG wiring is established (9). To determine where in the cell VALopA is localized, we stably overexpressed VALopA tagged with the fluorescent protein mKate2 under the UAS promoter in the 1020:Gal4 line *Tg(s1020t:Gal4; Cerulean:UAS:VALopA-mKate2)*. Live confocal imaging of the spinal cord revealed that VALopA-mKate2 localizes to protrusions into the spinal canal and short processes of lateral neurons (Fig. 1 *A* and *B* and *SI Appendix, Fig. S1A*). Since KA cells project motile cilia into the spinal canal (16, 17), we wondered whether VALopA targets to these cilia. Using a custom-built lattice light sheet microscope with adaptive

optics (18), we imaged *Tg(s1020t:Gal4; UAS:GCaMP5)* 1 dpf fish, in which Cerulean:UAS:VALopA was transiently expressed via DNA injection (*SI Appendix, Fig. S1C*). Fast (400 fps) imaging revealed that VALopA-mKate2-rich cilia are motile, oscillating at approximately 25 beats per second (*SI Appendix, Fig. S1D* and *Movie S1*).

To test VALopA localization more broadly in the organism, we injected capped RNA (cRNA) encoding HA-tagged VALopA into the 1-cell-stage zebrafish embryo, fixed embryos at ~24 hours post fertilization (hpf) and antibody stained for HA to visualize VALopA and for acetylated tubulin to mark cilia. VALopA co-localized with acetylated tubulin in KA cell cilia in the spinal canal (*SI Appendix, Fig. S1E, Top row*). It also co-localized with cilia in the eye and otic vesicle (*SI Appendix, Fig. S1E, Middle and Bottom rows, respectively*). To further verify ciliary localization of VALopA, we co-injected cRNAs encoding VALopA-mKate2 and the cilia marker Arl13b-GFP (19). Co-localization between these proteins confirmed VALopA targeting to KA cell motile cilia in the spinal canal and to primary cilia of lateral CPG neurons, as well as to primary cilia in the muscle cells that flank the spinal cord (Fig. 1 *E* and *F*). To assess the type and location of *valopa+* cells, we performed in situ hybridization on ~24 hpf fish. Single color in situ hybridization imaging on laterally and dorsally mounted fish revealed *valopa+* cells in the spinal cord, consistent with previous observations [*SI Appendix, Fig. S2A and B* and (11)]. Imaging of the dorsal-mount showed no *valopa+* cells abutting the spinal canal, thus endogenous *valopa* was not detected in KA cells

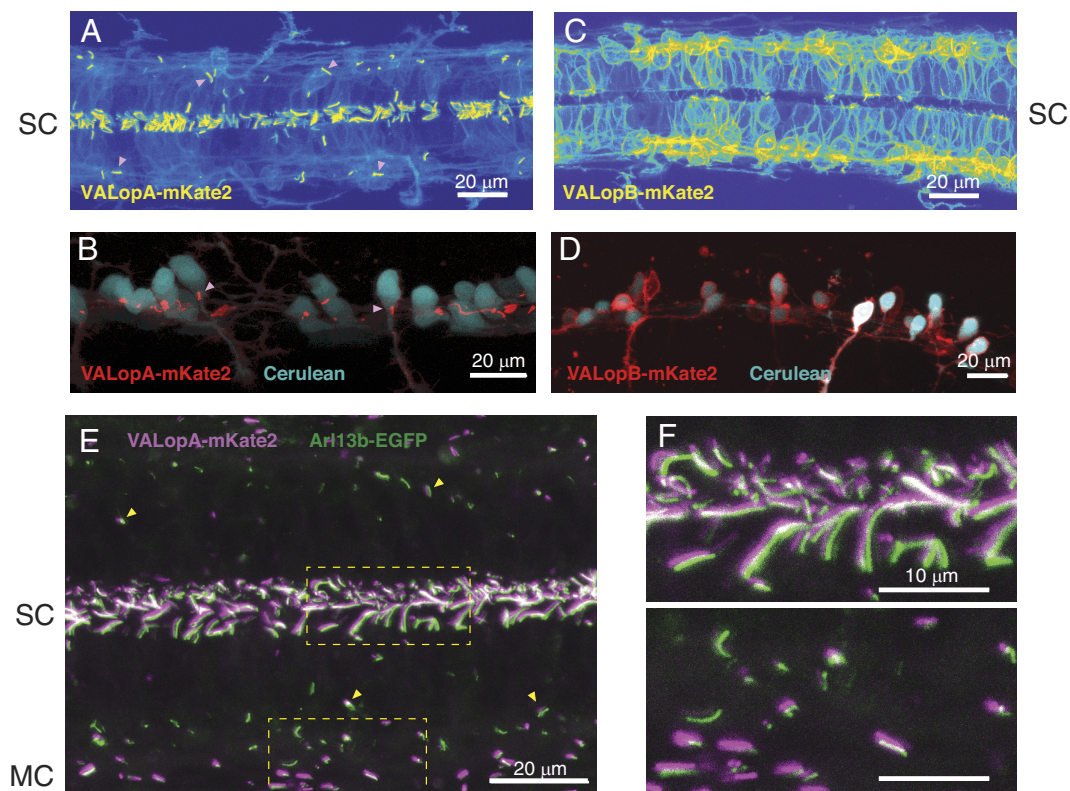


**Fig. 1.** Extraretinal opsins VALopA and VALopB localize to distinct subcellular compartments. (*A* and *B*) MIP images of the spinal cord of *Tg(s1020t:Gal4; Cer:UAS:VALopA-mKate2)* fish taken ~24 hpf. (*A*) Pseudo-color (by intensity) MIP of VALopA-mKate2 images taken from a dorsal mount. (Scale bar, 20  $\mu$ m.) SC = spinal canal. Pink arrows point to primary cilia in laterally located cells. Images are individually adjusted to saturate top 1% and bottom 1% of pixels. (*B*) MIP of Cerulean and VALopA-mKate2 images of the spinal cord taken from a lateral mount. (Scale bar, 20  $\mu$ m.) Pink arrows point to primary cilia on motor neurons. (*C* and *D*) MIP images of *Tg(s1020t:Gal4; Cer:UAS:VALopB-mKate2)* fish taken ~24 hpf. (*C*) Pseudo-color (by intensity) MIP image of VALopB-mKate2 images taken from a dorsal mount. (Scale bar, 20  $\mu$ m.) SC = spinal canal. Images are individually adjusted to saturate top 1% and bottom 1% of pixels. (*D*) MIP image of Cerulean and VALopB-mKate2 images of the spinal cord taken from a lateral mount. (Scale bar, 20  $\mu$ m.) (*E* and *F*) MIP images of the spinal cord of ~24-hpf fish expressing VALopA-mKate2 and Arl13b-EGFP via cRNA co-injection, from a dorsal mount. SC = spinal canal. MC = muscle cells. (Scale bar, 20  $\mu$ m.) Yellow arrows highlight cilia on laterally located cells. Yellow dashed rectangles denote zoomed images displayed in (*E*) showing motile cilia in the spinal canal (*Top*) and primary cilia on lateral cells (*Bottom*). (Scale bar, 10  $\mu$ m.) Chromatic aberration was left intact to highlight co-localization of VALopA-mKate2 and Arl13b-EGFP.

(*SI Appendix, Fig. S2B*). Next, we stained for *valopa* mRNA in *Tg(mnx:Gal4; UAS:GCaMP5)* fish, which express GCaMP5 in motor neurons [(12), *Materials and Methods*]. Two-color images showed *valopa* in both GCaMP5-positive motor neurons and GCaMP5-negative neurons (*SI Appendix, Fig. S2C*). Imaging of laterally mounted *Tg(s1020t:Gal4; Cerulean:UAS:VALopA-mKate)* confirmed that in motor neurons, identified by their ventral-reaching processes, VALopA targets to primary cilia (Fig. 1*B*). Targeting to primary cilia was also seen in transiently transfected cultured rat hippocampal neurons (*SI Appendix, Fig. S3A*). Thus, we find that VALopA functions from primary cilia in motor neurons and other lateral neurons in the CPG and that it targets to cilia in both fish and mammalian cells.

**VALopA Homolog VALopB Localizes to the Cell Body Plasma Membrane.** Zebrafish have a second vertebrate ancient long opsin, VALopB, which appears to be expressed outside of the CPG circuit (11) and, unlike VALopA, was not detected in RNAseq analysis of the 1020:Gal4 line that composes a core element of the CPG circuit (9). To test whether ciliary localization is conserved across these homologous opsins, we stably overexpressed VALopB-mKate2 in the 1020:Gal4 line *Tg(s1020t:Gal4; Cerulean:UAS:VALopB-mKate2)* and also injected cRNA encoding HA-tagged VALopB into the 1-cell-stage embryos. In contrast to VALopA, we found that VALopB localizes to the plasma membrane of neuronal cell bodies in the spinal cord, eye, and otic vesicle, with little expression in cilia (Fig. 1 *C* and *D* and *SI Appendix, Fig. S1 B* and *F*). VALopB also localized exclusively to the plasma membrane of the cell body in rat primary hippocampal neurons (*SI Appendix, Fig. S3B*). These results suggest that VALopA contains ciliary targeting motif(s) that VALopB lacks and that the comparison of VALopA to VALopB may offer insight into how ciliary localization versus cell body localization of a GPCR affects downstream behavior.

**Chimeras between VALopA and VALopB Identify Cilia-Targeting Motifs.** Before testing the behavior driven by the differently localized VALopA and VALopB, we wished to identify ciliary-targeting domain(s) contained within VALopA. We made a series of chimeras between VALopA and VALopB tagged with mKate2 and assessed their localization patterns in the spinal cord at ~24 hpf via cRNA overexpression. To set the boundaries of the intracellular loops between membrane-spanning segments and the boundaries of the termini, we aligned VALopA and VALopB (Fig. 2 *A* and *B* and *SI Appendix, Figs. S4* and *S5*) in reference to rhodopsin, which has a well-established crystal structure (*Materials and Methods*), and used the alignments to guide our boundary assignment. First, we endeavored to pull VALopA out of the cilium by replacing VALopA domains with those of VALopB. Since previous studies have uncovered ciliary targeting sequences (CTSs) in both the intracellular loop 3 (IL3) and the C-terminal tail of GPCRs (20–22), we transplanted the IL3 and C-terminal tail of VALopB onto VALopA separately and together. To quantify targeting, we generated maximum intensity projection (MIP) images of the spinal cord and counted the number of opsin-positive cilia in a defined region of the spinal cord to obtain a cilium density measurement (*Materials and Methods*).

VALopA whose IL3 domain was substituted with that of VALopB [“A(IL3-B)”] did not change in cilium density; however, VALopA whose C-terminus was substituted with that of VALopB [“A(Cterm-B)”] showed a small loss (>15%) of cilium density and increase in plasma membrane intensity (Fig. 2 *C* and *E*). Transplantation of both IL3 and the C-terminus of VALopB onto

VALopA [“A(IL3-B,Cterm-B)”] yielded lower cilium density, although the chimera was still partially ciliary. We surmised that other CTSs existed outside of the IL3 and C-terminus domains and transplanted additional VALopB domains onto VALopA to try to further remove it from the cilium. On top of the previous substitutions, we swapped the IL2 domain [“A(IL2-B,IL3-B,Cterm-B)”], which lowered cilium density further, and also generated a “full chimera,” [“A(Full Chimera)”], where the extracellular N-terminus and all intracellular domains were transplanted from VALopB onto VALopA, which had the lowest density of opsin positive cilia (Fig. 2 *C* and *E*). These observations confirm that CTSs exist outside of the IL3 and C-terminus. We also observed that substituting the C-terminal tail of VALopA for VALopB is sufficient to drive significant relocalization to the plasma membrane of the cell body (Fig. 2 *C* and *E*).

Next, we sought to bring VALopB to the cilium by transplanting domains from VALopA onto VALopB. We found that, individually, swapping the IL2 [“B(IL2-A)”], the IL3 [“B(IL3-A)”], or the C-terminal tail [“B(Cterm-A)”] of VALopA onto VALopB increased cilium density, whereas a swap of the N-terminus [“B(Nterm-A)”] or the IL1 [“B(IL1-A)”] did not (Fig. 2 *D* and *F*). A combined swap of the VALopA IL3 and C-terminus onto VALopB [“B(IL3-A,Cterm-A)”] had a similar effect as either individual swap (Fig. 2*F*). Taken together, the results suggest that motifs in the IL2, the IL3 and the C-terminal tail of VALopA contribute to its ciliary targeting. Markedly, the C-terminal tail of VALopA drives VALopB both into cilia and out of the cell body, whereas B(IL2-A) and B(IL3-A) maintain some expression in the cell body (Fig. 2*D*). Paired with the observation that the C-terminal tail of VALopB is sufficient to partially relocalize VALopA to the plasma membrane, we surmise that the C-terminal tail of VALopA is critical to ciliary targeting. With these chimeras in hand, we next assessed how subcellular localization affects signaling as read out by the CPG output to behavior.

**VALopB Substitutes for VALopA in Photo-Inhibition of Coiling.** Since VALopA localizes to the cilia, whereas VALopB stays in the cell body, we asked whether VALopB is capable of photo-inhibiting coiling, or whether photo-inhibition is a specific property of VALopA. To test the photo-inhibitory capabilities of VALopA and VALopB side-by-side, we designed two different overexpression/rescue systems that lacked endogenous *valopa*. First, we stably overexpressed either VALopA or VALopB in neurons of the CPG using UAS expression in the 1020:Gal4 fish line [*Tg(s1020t:Gal4; Cer:UAS:VALopA-mKate2)* or *Tg(s1020t:Gal4; Cer:UAS:VALopB-Kate2)*] and knocked-down endogenous *valopa* with a splice-blocking morpholino that interacts with endogenous but not transgenically expressed VALopA-mKate mRNA. Coiling behavior was assessed on a custom-build zBox, as previously described [Fig. 3*A* and (9, 23)]. Experiments were performed on forty-eight 22 to 24 hpf embryonic fish simultaneously, each in its own well, where fish were imaged in the dark under infrared illumination to monitor behavior without photo-activating VALopA or VALopB. For this experiment, embryos were dark-adapted overnight, imaged for 30-min to obtain a baseline measure of spontaneous coiling, and then the opsin was photo-activated with a 2-min pulse of 505-nm light (1.3 mW/cm<sup>2</sup>). Imaging continued for 60 to 90 min after the light pulse. As shown previously (9), the morpholino alone (in fish without VALopA-mKate2 or VALopB-mKate2 overexpression) eliminated photo-inhibition of coiling. Overexpression of VALopA-mKate2 [in *Tg(s1020t:Gal4; Cer:UAS:VALopA-mKate2)*] in a morpholino-injected animal restored photo-inhibition (*SI Appendix, Fig. S6A*).

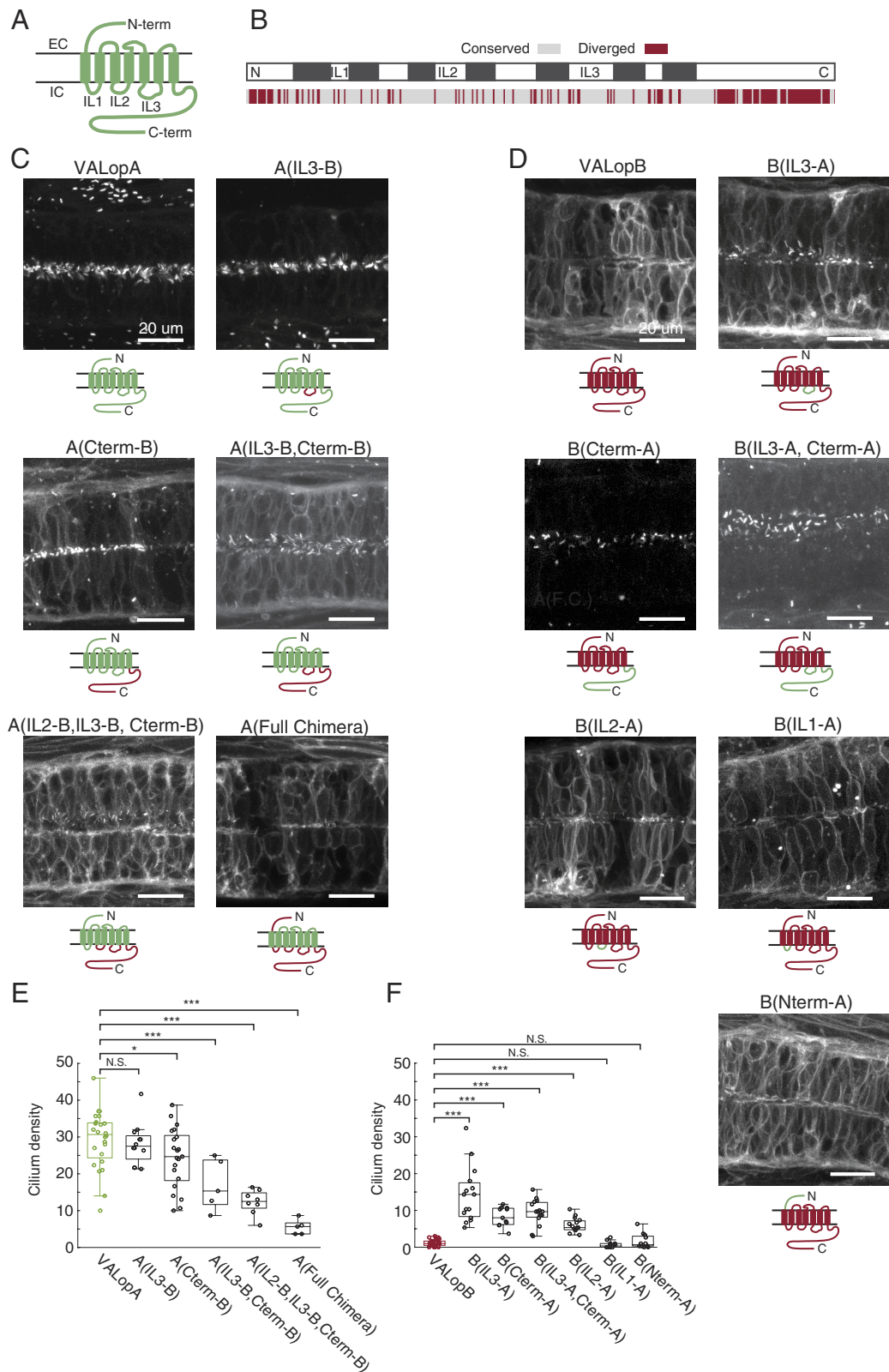


**Fig. 2.** Cytoplasmic domains of VALopA and VALopB mediate cilia and cell body targeting. (A) Schematic of the canonical 7-transmembrane G-protein-coupled receptor. (B) AA alignment of VALopA and VALopB with domains delineated, 67% identity (gray = conserved AAs, maroon = diverged AAs) (Right). (C and D) MIP live images of the spinal cord of ~25 hpf fish expressing VALopA or its chimeras (C) or VALopB or its chimeras (D) with accompanying schematic showing the opsin identity below each image. All opsins are tagged with mKate2 for visualization. The maximum pixel value has been manually adjusted for each image. (Scale bar is 20  $\mu$ m.) (E and F) Quantification of cilium density (cilium counts in a 30- $\mu$ m lateral section of the spinal cord) for VALopA and its chimeras (E) and VALopB and its chimeras (F). Each data point represents quantification of a single fish. VALopA: n = 24, A(IL3-B): n = 12, A(Cterm-B): n = 21, A(IL3-B, Cterm-B): n = 5, A(IL2-B, IL3-B, Cterm-B): n = 8, A(Full Chimera): n = 5, VALopB: n = 30, B(Nterm-A): n = 12, B(IL1-A): n = 12, B(IL2-A): n = 15, B(IL3-A): n = 15, B(Cterm-A): n = 11, B(IL3-A, Cterm-A): n = 15; significance is tested against the parent protein using the Wilcoxon rank sum test, \* $P < 0.05$ , \*\* $P < 0.01$ , \*\*\* $P < 0.001$ .

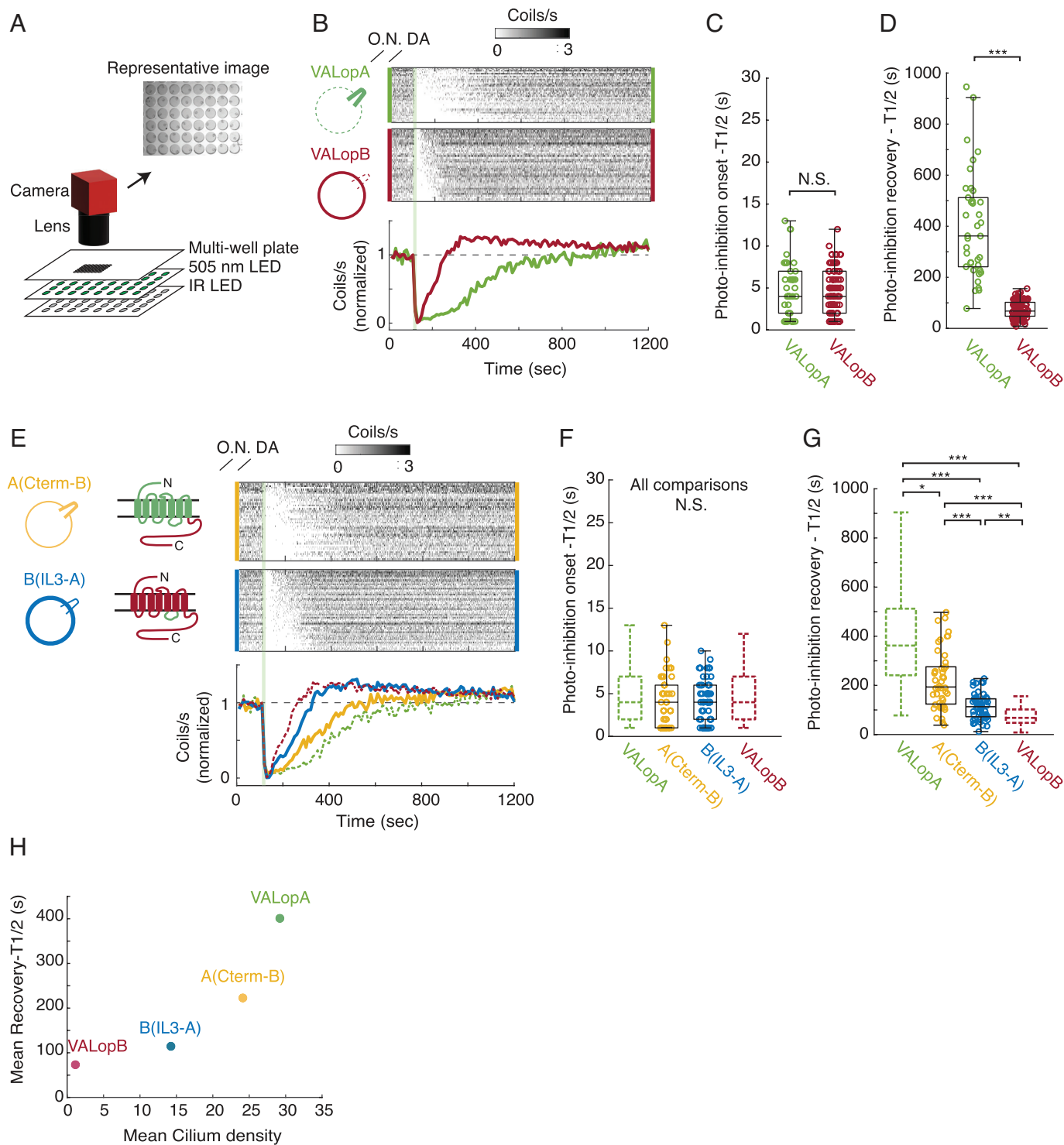


**Fig. 3.** Distinct behavioral kinetics of VALopA, VALopB, and chimera-dependent photo-inhibition. (A) Schematic of semi-high throughput behavioral imaging of 1 dpf zebrafish embryos on the zBox. (B) Light-dependent inhibition of coiling for VALopA (green,  $n = 38$ ) or VALopB (red,  $n = 81$ ) overexpressed in *valopa*<sup>-/-</sup> fish via cRNA injection. Light protocol: single 15-s, 505-nm pulse; overnight dark adaptation (O.N. DA) precedes imaging run. Light pulse is shown as a shaded green line. Single fish coiling rate heat maps (Top) and mean traces (Bottom) are shown. Fish are pooled from multiple experiments. For the VALopB coiling rate heat map, only every other fish is shown for brevity. Schematic showing opsins' localization patterns shown on Left. (C and D) Quantification of photo-inhibition onset (T1/2) (C) and recovery (T1/2) (D) from coiling data shown in (B). Significance is calculated using the Wilcoxon rank sum test, \* $P < 0.05$ , \*\* $P < 0.01$ , \*\*\* $P < 0.001$ . (E) Light-dependent inhibition of coiling for A(Cterm-B) (yellow,  $n = 46$ ) and B(IL3-A) (blue,  $n = 57$ ) overexpressed in *valopa*<sup>-/-</sup> fish via cRNA injection. Light protocol: single 15-s, 505-nm pulse; overnight dark adaptation (O.N. DA) precedes imaging run. Light pulse is shown as a shaded green line. Single fish coiling rate heat maps (Top) and mean traces (Bottom) are shown. Schematic showing opsins' identity and localization patterns shown on Left. Fish are pooled from multiple experiments. VALopA (green, dashed) and VALopB (red, dashed) from (B) is shown as well. (F and G) Quantification of photo-inhibition onset (T1/2) (F) and recovery (T1/2) (G) from coiling data shown in (E). Data from previous panels is replicated as dashed boxplots lacking single data points. Significance is calculated using the Kruskal-Wallis test followed by a multiple comparisons test, \* $P < 0.05$ , \*\* $P < 0.01$ , \*\*\* $P < 0.001$ . (H) Mean cilium density was plotted against mean recovery (T1/2) values for VALopA, VALopB, A(Cterm-B), and B(IL3-A). Mean values are derived from (D) and (G) and from Fig. 2 E and F.

Overexpression of VALopB-mKate2 [in *Tg(s1020t:Gal4; Cer:UAS:VALopB-mKate2)*] also restored photo-inhibition in the VALopA morpholino knockdown (*SI Appendix, Fig. S6B*), indicating that VALopB functions similarly to VALopA in CPG neurons.

Second, we performed rescue experiments with global overexpression via cRNA injection in CRISPR/Cas9 *valopa* knockout animals. To generate *valopa*<sup>-/-</sup> fish, one-cell-stage embryos were co-injected with Cas9 mRNA and the guide RNA (sgRNA) TCAGAGACACCAGGAAGT designed to target the first exon of the *valopa* (NM\_131586) gene. One-day-old embryos were screened for diminished photo-inhibition on the zBox and raised (*SI Appendix, Fig. S7A*). Some F1 progeny of potential founders yielded no photo-inhibition (*SI Appendix, Fig. S7B*). Genotyping of photo-insensitive F1 fish revealed 19 different mutant alleles (*SI Appendix, Fig. S7C*). Like the morpholino-driven VALopA knockdown, *valopa*<sup>-/-</sup> fish displayed no 505-nm light-dependent photo-inhibition in 22 to 24 hpf embryos, whereas *valopa*<sup>+/-</sup> heterozygous embryos maintained photo-inhibition (*SI Appendix, Fig. S7 B and D*). Starting at 25 hpf, *valopa*<sup>-/-</sup> fish exhibited a transient phase of stimulation by light (photo-motor response) (*SI Appendix, Fig. S7D*), as shown earlier to persist in the VALopA morpholino knockdown (9, 24).

We injected *valopa*<sup>-/-</sup> animals with VALopA or VALopB cRNA, subject them to an overnight dark adaptation followed by a 15-s, 505-nm light pulse, and found that global overexpression of VALopA or VALopB in a *valopa* knockout background was able to effectively photo-inhibit coiling, consistent with the data obtained from the CPG-circuit specific expression with morpholino *valopa* knockdown (Fig. 3B). These data confirm that cell body-localized VALopB is able to modulate the same behavior as cilia-localized VALopA.

**VALopB Differs in Signaling Kinetics from VALopA.** Given that the ability of these opsins to photo-inhibit coiling is not dependent on their subcellular localization, we then asked whether cilia-localized VALopA and cell body-localized VALopB photo-inhibited with different kinetics. We performed kinetic analysis of the overexpression rescue experiments and extracted onset and recovery rates from single fish traces. We found that for both types of rescue experiments, fish that overexpressed VALopA or VALopB experienced similar rates of onset of photo-inhibition [“Photo-inhibition onset (T<sub>1/2</sub>)”] (Fig. 3C and *SI Appendix, Fig. S6C*). However, VALopA-expressing fish recovered from photo-inhibition of coiling [“Photo-inhibition recovery (T<sub>1/2</sub>)”] more slowly than VALopB-expressing fish, taking over twice as long to return to half of baseline coiling rates (Fig. 3D and *SI Appendix, Fig. S6D*).

**Ciliary Targeting Slows Kinetics of Coiling Behavior Photo-Inhibition.** Given that cilia-localized VALopA signals with slower kinetics than cell body-localized VALopB, we wondered whether GPCRs in the cilia elicit prolonged signals following a pulse of activation. To address this, we asked how removing VALopA from the cilium or retargeting VALopB to the cilium would change their impact on coiling behavior. We went about this in two ways, using VALopA/VALopB chimeras and using ciliary VALopB fusion proteins to generate these comparisons. Given the difficulty in fully removing VALopA from the cilium, we compared the wholly ciliary VALopA to chimeric VALopA with the C-terminal tail of VALopB [A(Cterm-B)], which we found to have reduced ciliary expression and more cell body expression (Fig. 2 C and E). We also compared the cell

body-localized VALopB to chimeric VALopB with the IL3 of VALopA [B(IL3-A)], which has more ciliary expression (Fig. 2 D and F). If cilia-targeted GPCRs signaled for longer, we would expect VALopA to recover from photo-inhibition more slowly than A(Cterm-B) and for B(IL3-A) to recover from photo-inhibition more slowly than VALopB. We overexpressed these chimeras via cRNA injection in *valopa*<sup>-/-</sup> fish and performed behavioral imaging using the overnight dark adaptation and 15-s light pulse protocol at 22 to 24 hpf. We found that A(Cterm-B) and B(IL3-A) expressed well and rescued photo-inhibition in zebrafish embryos (Figs. 2 C and D and 3E). Though onset rates for all opsins were statistically equivalent, the recovery from photo-inhibition was accelerated in the A(Cterm-B) rescue relative to the VALopA rescue and decelerated in the B(IL3-A) rescue relative to the VALopB rescue (Fig. 3 E–G), in accordance with our predictions above. The positive correlation between ciliary expression and photo-inhibition length is further illustrated by plotting the mean cilium density measurement against mean recovery rate for each opsin (Fig. 3H).

To examine the role of ciliary targeting in behavioral kinetics further, we took another approach to retarget the opsins. Using two distinct ciliary-localizing proteins, we generated a suite of VALopB fusion proteins with differing subcellular localization patterns. First, we C-terminally tagged VALopB with either Arl13b [“B-Arl13b”], which has been shown to relocalize GPCRs to cilia or Arl13b(V358A) [“B-Arl13b(PM)”], which has been shown to stay in the cell body (5). As expected, B-Arl13b targeted to cilia and B-Arl13b(PM) remained in the cell body in the spinal cord, eye, and otic vesicle of the one-day-old zebrafish (Fig. 4A and *SI Appendix, Fig. S8 A and B*). We then compared the photo-inhibition behavioral kinetics of these two VALopB fusion proteins via cRNA injection in *valopa*<sup>-/-</sup> using the overnight dark adaptation, 15-s light pulse protocol at 22 to 24 hpf. We found that the cilia-targeted VALopB fusion, B-Arl13b had slower kinetics of photo-inhibition onset and recovery than the cell body-localized B-Arl13b(PM) (Fig. 4 B–D). Second, we C-terminally tagged VALopB with constitutively active Rab23 [VALopB-Rab23(Q68L), “B-Rab23(CA)”], which was previously shown to target GPCRs to cilia (22). We found that B-Rab23(CA) localized to cilia in the spinal cord, eye, and otic vesicle of the one-day-old fish (Fig. 4E and *SI Appendix, Fig. S8C*). We then overexpressed B-Rab23(CA) via cRNA injection in *valopa*<sup>-/-</sup> fish and performed behavioral imaging using the overnight dark adaptation, 15-s light pulse protocol at 22 to 24 hpf. Comparing photo-inhibition kinetics between ciliary B-Rab23(CA) and cell body-localized VALopB, we find that onset rates for the two opsins are statistically equivalent, but recovery for the B-Rab23 opsins is significantly longer than for VALopB (Fig. 4 F–H). We also C-terminally tagged VALopB with dominant negative Rab23 [VALopB-Rab23(S23N), “B-Rab23(DN)”], to control for the effect of Rab23 activity on subcellular localization and photo-inhibitory behavior. We also found that B-Rab23(DN), although noted to have a limited ability to target GPCRs to cilia (22) still achieves ciliary targeted at high cRNA injection concentrations (~200 ng/μL), with lower ciliary expression relative to B-Rab23(CA) (*SI Appendix, Fig. S9 A–C*). Overexpression and activation of B-Rab23(DN) with the same protocol described above demonstrate that B-Rab23(DN), too, recovers from photo-inhibition more slowly than VALopB (*SI Appendix, Fig. S9 D–F*). As a whole, our findings using VALopB and ciliary protein fusions mirror our earlier findings in chimeric opsins. Thus, using two orthogonal approaches, we find that retargeting these opsins to the cilium slows recovery kinetics and retargeting these opsins to the cell body speeds recovery kinetics.

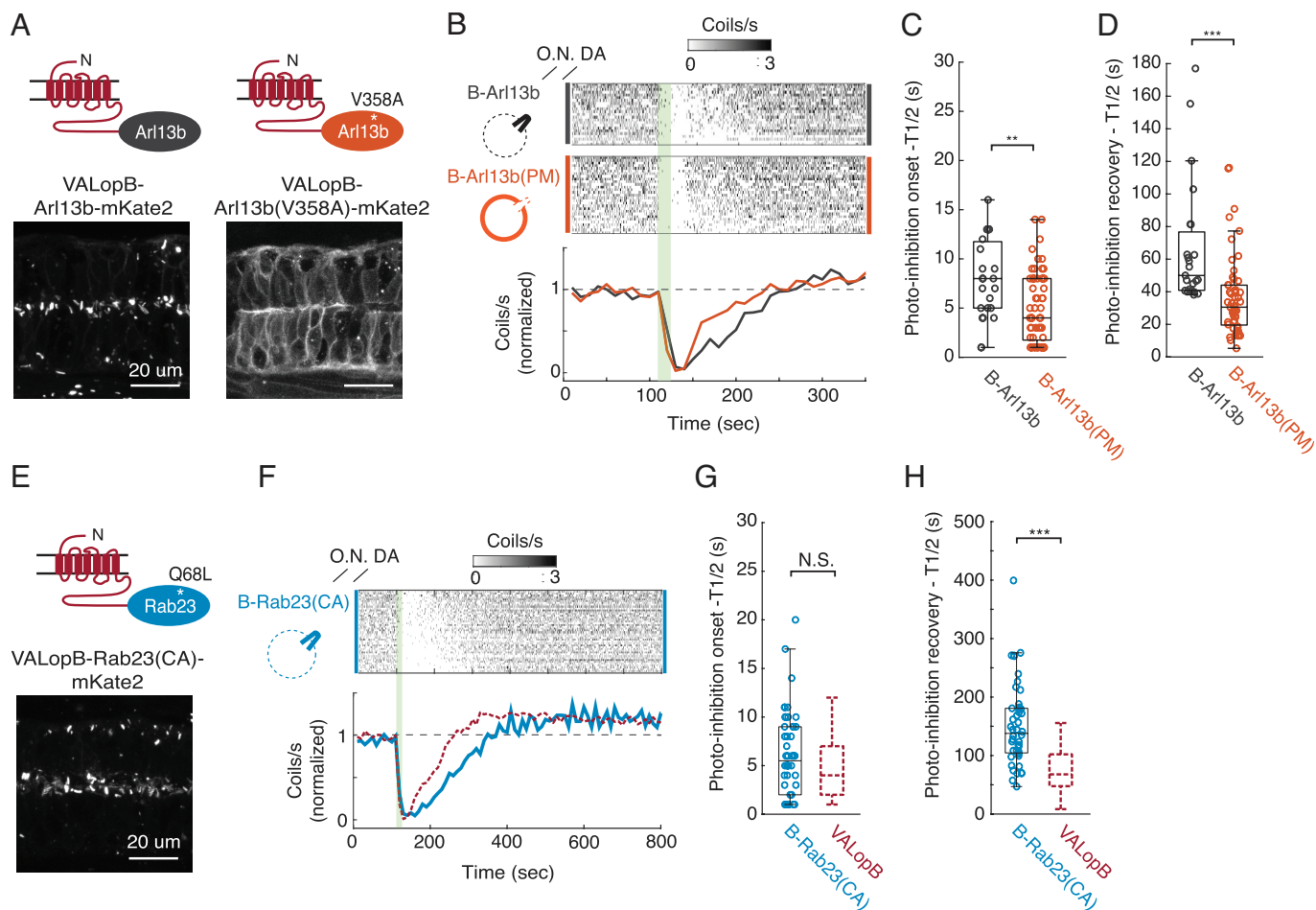


**Fig. 4.** Ciliary VALopB fusion proteins induce VALopA-like slow photo-inhibition. (A) Schematic of opsin (Top) and MIP images (Bottom) of the spinal cord of the ~24 hpf fish with overexpressed VALopB-Arl13b-mKate2 (Left) or VALopB-Arl13b(V358A)-mKate2 [Arl13b(PM)] (Right) via cRNA injection in ~24 hpf fish. (Scale bar, 20  $\mu$ m.) (B) Light-dependent inhibition of coiling for B-Arl13b (black, n = 23) and B-Arl13b(PM) (orange, n = 57) overexpressed in *valopa*<sup>-/-</sup> fish via cRNA injection. Flash protocol: single 15-s, 505-nm pulse; overnight dark adaptation (O.N. DA) precedes imaging run. Light pulse is shown as a shaded green line. Single fish coiling rate heat maps (Top) and mean traces (Bottom) are shown. Fish are pooled from multiple experiments. For the B-Arl13b(PM) coiling rate heat map, only every other fish is shown for brevity. Schematic showing opsins' localization patterns shown on Left. (C and D) Quantification of photo-inhibition onset (T1/2) (C) and recovery (T1/2) (D) from coiling data shown in (B). Significance is calculated using the Wilcoxon rank sum test, \**P* < 0.05, \*\**P* < 0.01, \*\*\**P* < 0.001. (E) Schematic of opsin (Top) and MIP images (Bottom) of the spinal cord of ~24 hpf fish with overexpressed VALopB-Rab23(Q68L)-mKate2 [constitutively active Rab23-Rab(CA)] via cRNA injection. (Scale bar, 20  $\mu$ m.) (F) Light-dependent inhibition of coiling for B-Rab23(CA) (cerulean, n = 46) overexpressed in *valopa*<sup>-/-</sup> fish via cRNA injection. Light protocol: single 15-s, 505-nm pulse; overnight dark adaptation (O.N. DA) precedes imaging run. Light pulse is shown as a shaded green line. Single fish coiling rate heat maps (Top) and mean traces (Bottom) are shown. Fish are pooled from multiple experiments. Schematic showing opsins' localization patterns shown on Left. VALopB (red, dashed) from Fig. 3B is shown as well. (G and H) Quantification of photo-inhibition onset (T1/2) (G) and recovery (T1/2) (H) from coiling data shown in (F). VALopB data from Fig. 3C and D is shown as dashed boxplots lacking single data points. Significance is calculated using the Wilcoxon rank sum test, \**P* < 0.05, \*\**P* < 0.01, \*\*\**P* < 0.001.

### Intrinsic Signaling Kinetics of Opsins in a Cilia-Free System.

In order to assess the intrinsic signaling kinetics of VALopA and VALopB, independent of their subcellular localization, we measured their activation of an ion channel in *Xenopus* oocytes, which lack a primary cilium. We previously showed that a flash of light to oocytes expressing VALopA and the GIRK1 and GIRK2 subunits of the G-protein-activated inward-rectifying potassium channel activates K<sup>+</sup> current, indicating that VALopA is G<sub>i</sub> coupled [Fig. 5A and (9)]. Here, we expressed either VALopA or VALopB in *Xenopus* oocytes along with GIRK1 and GIRK2 and assessed their signaling kinetics via GIRK current. Two-electrode voltage clamp recordings showed that brief (10 to 100 ms long) flashes of light at 488-nm (40-nm bandpass) robustly activate GIRK current with both VALopA and VALopB (Fig. 5B), indicating that, like VALopA, VALopB also couples to G<sub>i</sub>. We found that VALopA activation of GIRK channels has slower on and off kinetics than VALopB (Fig. 5C and D). We therefore asked whether the kinetic differences displayed by our retargeted

chimeras and fusion proteins were due to differences in subcellular localization or intrinsic signaling. We found no statistically significant difference in GIRK current kinetics between VALopA and its more cell body localized chimera A(Cterm-B) or between VALopB and its cilia-targeted fusion proteins B-Arl13b or B-Rab(CA) (Fig. 5E–J). These results suggest that the differences in behavioral kinetics seen in zebrafish between the retargeted GPCRs and their parent proteins are due to subcellular localization and not intrinsic signaling differences. Of note, VALopA's intrinsically slower kinetics likely contributes to its slow recovery observed in our zebrafish behavioral assay, which may explain why the slow recovery observed in the ciliary VALopB opsins rescue system falls short of the slow recovery observed in the VALopA rescue.

**Ciliary Localization Amplifies Opsin Signaling Strength.** We also wished to test how the unique signaling environment of the primary cilium affects the strength of the GPCR signal emanating from the cilium. We observed that retargeting a cell



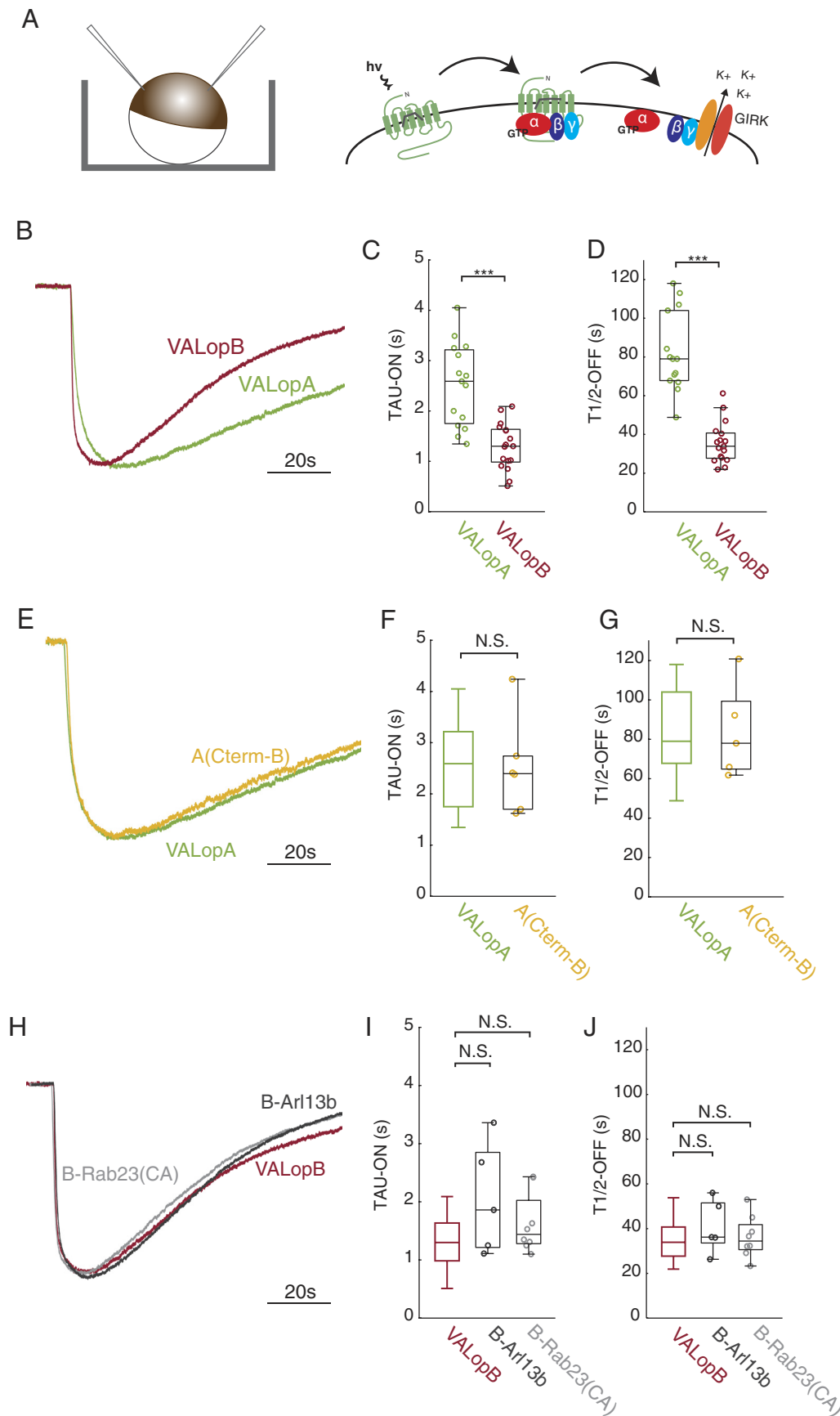


**Fig. 5.** Electrophysiological recordings in a cilia-free system assess intrinsic signaling kinetics. (A) Model of opsin activation leading to GIRK current. (B) Representative normalized traces of VALopA or VALopB activated GIRK current in response to a light flash in oocytes. (C and D) Quantification of TAU-ON (C) and T1/2-OFF (D) rates (VALopA: n = 14, VALopB: n = 17). (E) Representative, normalized traces of VALopA (from B) or A(Cterm-B) activated GIRK current in response to a light flash in oocytes. (F and G) Quantification of TAU-ON (F) and T1/2-OFF (G) rates [A(Cterm-B) n = 5]. (H) Representative, normalized traces of VALopB (from B) B-Rab23(CA), and B-Arl13b activated GIRK current in response to a light flash in oocytes. (I and J) Quantification of TAU-ON (I) and T1/2-OFF (J) rates (B-Rab23(CA): n = 8, B-Arl13b: n = 5). Data from previous panels are replicated as boxplots lacking single data points. Significance is calculated using the Wilcoxon rank sum test, \* $P < 0.05$ , \*\* $P < 0.01$ , \*\*\* $P < 0.001$ .

body-localized GPCR to the primary cilium appears to greatly decrease its total expression (Fig. 2), and yet our opsins are still able to signal effectively from the primary cilia. To test an

amplification hypothesis, we compared the relative expression and photo-inhibition strength of cell body-localized VALopB to a ciliary-localized chimera B(IL3-A, Cterm-A) ["B-Cil"] (Fig. 6A).

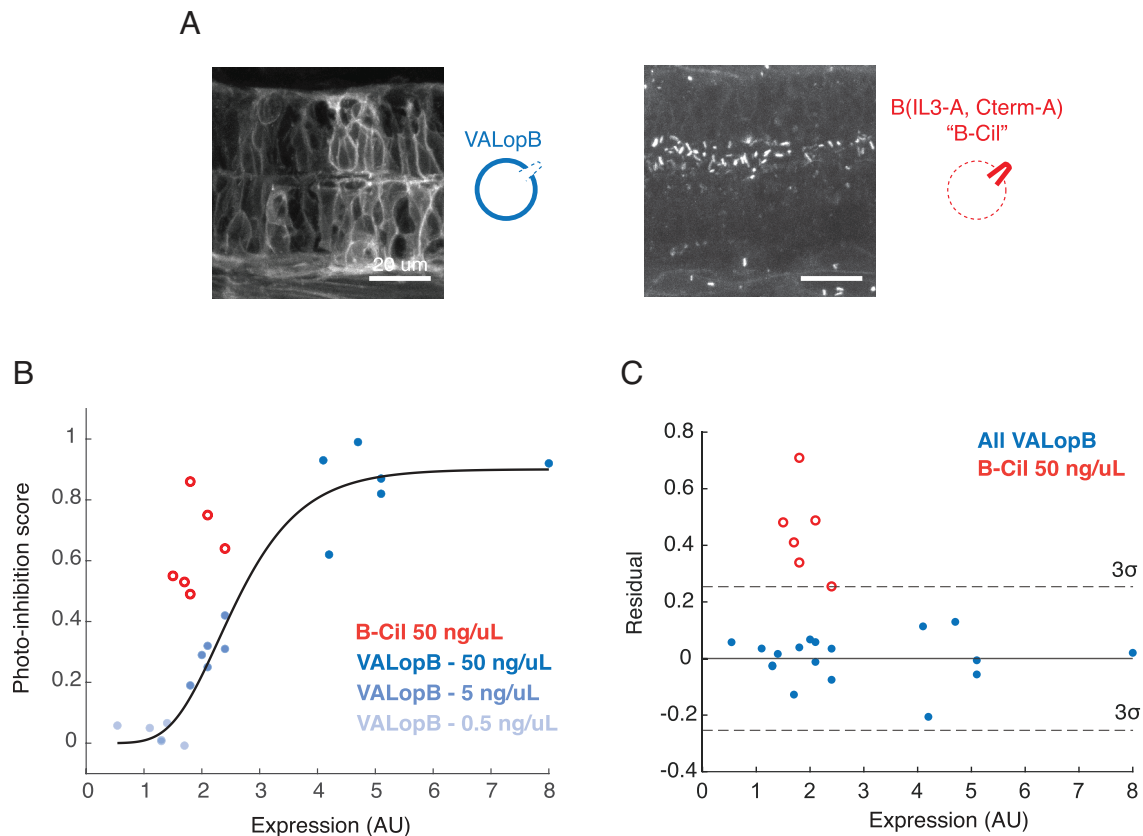


**Fig. 6.** VALopB signaling is amplified in the primary cilium. (A) MIP images of VALopB (Left) and B(IL3-A, Cterm-A) (Right), termed "B-Cil", replicated from Fig. 2D. Schematics showing opsins' expression patterns to right of images. (B) Plot of expression (AU) versus photo-inhibition score (PI) for 50 ng/ $\mu$ L mRNA injected B(IL3-A, Cterm-A) ("B-Cil"; red) and for 50 ng/ $\mu$ L (dark blue), 5 ng/ $\mu$ L (blue), and 0.5 ng/ $\mu$ L (light blue) mRNA injected VALopB. VALopB points were fit with a sigmoidal curve (black,  $R^2 = 0.95$ ). (C) Residuals from sigmoidal fit in (B) for VALopB fall within 3 SDs (dashed lines) from the distribution fit and for B-Cil (red) fall outside of 3 SDs from the distribution fit. Light protocol: single 2-min, 505-nm pulse; 10-min dark adaptation precedes imaging run used to obtain PI measurements.

To assess photo-inhibition strength, we overexpressed VALopB or B-Cil using cRNA injection in *valopa*<sup>-/-</sup> fish and subjected 22 to 24 hpf embryos to a 10-min dark adaptation followed by a 2-min 505-nm pulse of light. A photo-inhibition score (PI) was calculated as previously described [(9), *Materials and Methods*, and *SI Appendix, Fig. S7A*]. Following behavioral imaging, the fish were individually mounted and imaged to obtain quantitative measurements of opsin expression in the spinal cord (*Materials and Methods*). Given the higher expression of VALopB relative to B-Cil, we titrated down the amount of VALopB injected to obtain a range of expression and PI measurements. Strikingly, the expression vs. PI curve is well fitted by a sigmoidal curve (Fig. 6B,  $R^2 = 0.95$ ). The expression vs PI measurements for B-Cil fall to the left of the VALopB fitted curve, and outside of the distribution of residuals (Fig. 6C), showing that B-Cil evoked higher magnitude photo-inhibition (by ~two-to-three fold) of coiling for the same amount of protein expression.

We wondered whether enhanced photo-inhibition was due to stronger signaling in the cilium or to an intrinsic property of the pieces of VALopA that were transplanted into VALopB. We examined this by comparing the activation of GIRK channels by VALopB versus B-Cil in the cilia-free system of the *Xenopus* oocyte. Following a 5-min period of dark adaptation, a 5-ms light pulse elicited GIRK currents that were statistically indistinguishable between VALopB and B-Cil, (VALopB:  $243 \pm 50$  nA, B-Cil:  $289 \pm 54$  nA [mean  $\pm$  SEM];  $P > 0.2$  unpaired *t* test; *SI Appendix, Fig. S10A*). This indicates that VALopB and B-Cil have similar intrinsic signaling strength and supports the interpretation that higher inhibition of zebrafish coiling is due to ciliary targeting.

To test this further, we also compared expression versus photo-inhibition strength in the coiling embryo using Arl13b to retarget VALopB to cilia. We found that for equivalent expression (B-Arl13b—50 ng/ $\mu$ L mRNA and B-Arl13b(PM)—5 ng/ $\mu$ L mRNA), the ciliary B-Arl13b photo-inhibits more strongly than does the somatic B-Arl13b(PM) mutant (*SI Appendix, Fig. S10B*). Taken as a whole, these findings indicate that ciliary localization of these opsins prolongs and increases the strength of signaling.

## Discussion

In this study, we show that two related extraretinal opsins, when expressed in the zebrafish spinal cord CPG circuit for locomotion, modulate early locomotor coiling behavior with distinct kinetics. We find that VALopA is expressed in laterally located neurons of the locomotory CPG circuit and in motor neurons, suggesting that motor neurons also have the ability to sense their environment. We find VALopA targets to both primary and motile cilia in zebrafish spinal cord neurons, as well as to primary cilia in zebrafish muscle and cultured primary rat hippocampal neurons. In contrast, a homolog, VALopB, targets to the cell body. We characterize the molecular determinants of this targeting and show that the IL2, IL3, and C-terminal domains of VALopA contain CTSs. Although CTSs in the IL3 and C-terminus of other GPCRs have been identified, we are unaware of a prior example of a CTS in a GPCR outside of these two domains. Combined with the observation that VALopA with the IL2, IL3, and C-terminal tail of VALopB maintains some ciliary localization, the observations suggest that VALopA has evolved multiple, redundant CTSs to

ensure localization to cilia, suggesting that such localization may be important for its function.

We find that light-suppression of locomotor behavior through VALopA has slower kinetics than that elicited by VALopB, even though both are G<sub>i</sub>-coupled. To understand the functional impact of ciliary targeting, we studied chimeras between VALopA and VALopB that retarget VALopA to the cell body and VALopB to the cilium, as well as fusions between VALopB and ciliary proteins that retarget VALopB to the cilium. Retargeting VALopA to the cell body speeds recovery from locomotory photo-inhibition and targeting VALopB to the cilium slows recovery from photo-inhibition, indicating that ciliary targeting is a key determinant to signaling dynamics. Ciliary targeting also increased the magnitude of photo-inhibition by VALopB, thus revealing two forms of signal amplification by the ciliary compartment: duration and amplitude. VALopA signaling kinetics were also slower in *Xenopus* oocytes, which lack cilia, indicating that VALopA signaling is intrinsically slower than that of VALopB. Thus, the combination of ciliary localization of VALopA along with its intrinsically slow signaling kinetics produces a larger and longer-lasting regulation of neural circuit output in response to light.

Our observations pose the question: How does ciliary localization of a GPCR affect signaling? In the plasma membrane, the kinetics of opsin activation and deactivation/desensitization is shaped by its lipid micro-environment, by regulator of G-protein signaling (RGS) proteins, which turn off G-protein signaling, and by  $\beta$ -arrestin induced desensitization and internalization (25–27). It is an open question whether these factors operate differently in the primary cilium. The ciliary membrane has a distinct lipid and cholesterol profile compared to the cell body plasma membrane (28, 29), which might modify the lifetime of opsin signaling (30). It is also possible that the mechanisms that turn off the receptor or its downstream effectors are present in lower amounts in the cilium or recruited more slowly to the cilium. Indeed,  $\beta$ -arrestin 2 traffics from the cell body to the primary cilium of neurons following activation of SSTR3 in cilia (31). Additionally, the dynamics of signaling to downstream effectors may also be slower in the cilium.

A recent study discovered that the primary cilium can serve as a postsynaptic, axonal target that signals using the classical small molecule neurotransmitter serotonin (8), leading to the regulation of epigenetic programming in the nucleus. We also find that the cilium serves as a specialized signaling compartment: as an amplifying light-controlled regulator of neural activity that is potent enough to produce a protracted signal to turn off locomotor circuit output.

## Materials and Methods

**Embryo Collection and Injection.** All animal care and experiments were in accordance with the University of California at Berkeley Animal Care and Use Committee guidelines. Embryos were collected and injected with ~1 nL of 100 to 200 ng/ $\mu$ L cRNA (transient, whole-fish expression) or ~1 nL of 100 ng/ $\mu$ L DNA with 25 to 50 ng/ $\mu$ L tol2 cRNA (creation of transgenic fish lines) or 0.5 mM VALopA splice-blocking morpholino [TTGTGAAGACCTTCTGAGTTGC, Gene Tools (9)] at the one-cell-stage. All embryos were kept in E3 (300 mg/L Instant Ocean) with methylene blue. Injected embryos were raised in a dark, temperature-controlled incubator (28.5 °C) to prevent exogenous opsin activation during development. When needed, after the embryos reached the 60% epiboly stage, the temperature was lowered to 23.5 °C to 25 °C in order to delay development and enable timed experiments the following morning.

**Behavioral Imaging and Analysis.** A custom-made zBox was used (23) for all behavioral zebrafish experiments. Coiling experiments were performed on embryonic zebrafish aged 22 to 25 hpf in order to maximize coiling rates but minimize the presence of the photo-motor response (9, 24). Behavioral experiments were performed as described earlier (9). Briefly, imaging was performed

on the zBox on embryos placed individually in 48 wells (6  $\times$  8 well portion) of a clear-bottomed 384-well plate (Jarden) with two LED arrays placed below (505 nm and 940 nm, Mouser) for stimulation and imaging, respectively. Embryos were loaded either the night before or 30-min before initiation of imaging run for the overnight or 30-min dark adaptation periods. Coiling behavior for each fish was analyzed using a custom-built MATLAB script (9) that calculates the difference in pixel intensity between frames. Subsequent analysis was performed using custom-built MATLAB scripts. To obtain photo-inhibition onset and recovery parameters from zebrafish coiling data, the traces were first subject to a moving mean smoothing function. Photo-inhibition onset (T1/2) was obtained by detecting the timepoint at which the smoothed trace dipped below 1/2 of baseline (prelight pulse) coiling rates, relative to the start of the light pulse. Photo-inhibition recovery (T1/2) was obtained by fitting the smoothed, recovery portion of the trace to a single exponential function, extracting the t1/2 parameter, and adding the time between the end of the pulse and the start of the fit. Baseline coiling rates were obtained by averaging coiling rate per fish over the 48-min time window preceding light pulse. Baseline coiling was unaffected by expression in *valopa*<sup>-/-</sup> knockout fish of VALopA or VALopB, chimeric or ciliary protein fusion constructs, except to a small degree by VALopB-Rab23(CA) (*SI Appendix, Fig. S11*). Photo-inhibition scores (PI) were calculated using previous methods: [HzLight - HzDark]/HzDark (9). HzDark window was 2-min. Fig. 6B and *SI Appendix, Fig. S7 A and B* used an HzLight window of 2-min, whereas *SI Appendix, Fig. S10B* used an HzLight window of 20-s due to the shorter inhibitory kinetics of the Arl13b tagged VALopB's.

**Cellular Imaging.** Most cellular imaging was performed on a Zeiss LSM 880 NLO Axio Examiner upright confocal using a Zeiss Objective W Plan Apochromat 20x/1.0 DIC M27 75-mm water immersion objective and the 488, 561, 594, and 633 laser lines. For in vivo imaging, embryonic fish were manually removed from their chorion using sharp tweezers, mounted laterally in 1.4% agarose (UltraPure LMP Agarose, low melting point, Invitrogen, 16520) in E3 in 50-mm glass bottom dishes (MatTek, P50G-1.5-14-F) then paralyzed with 2 mg/mL alpha-bungarotoxin (Thomas Scientific) injected into the tail. Fixed and stained fish were mounted laterally in agarose without alpha-bungarotoxin injection. All fish were then mounted in a dorsal position for top-down imaging and imaged in E3 buffer. Live primary hippocampal neurons were imaged in extracellular buffer (135 NaCl, 5.4 KCl, 2 CaCl<sub>2</sub>, 1 MgCl<sub>2</sub>, and 10 HEPES, pH 7.4). For imaging on the custom-built lattice light sheet with adaptive optics, embryo injection and preparation for mounting in agarose were performed as described above. Then, 1 dpf embryos mounted dorsally in agarose were placed on an angular holder and imaged as described in ref. 18.

**Generation of Transgenic Fish Lines.** Creation of *Tg(s1020:Gal4; Cer:UAS:VALopA-mKate2)* and *Tg(s1020:Gal4; Cer:UAS:VALopA-mKate2)* lines: AB fish containing the 1020:Gal4 transgene were in-crossed and the embryos collected and injected with DNA (Cerulean:UAS:VALopA-mKate2 or Cerulean:UAS:VALopB-mKate2) with tol2 transposase cRNA at the one-cell-stage as described above. Fish were screened for CFP fluorescence at 1 dpf and raised. F1 transgenic fish were obtained by in-crossing potential founders (F0) and raising CFP-positive fish. Creation of *Tg(mnx:Gal4; UAS:Kaede)* line: AB fish containing the UAS:Kaede transgene (15) were in-crossed and the embryos collected and injected with DNA [mnx:Gal4, (32)] with tol2 transposase cRNA at the one-cell-stage. Fish were screened for Kaede (green) fluorescence at 1 dpf and raised. F1 transgenic fish were obtained by out-crossing potential founders with AB wild-type fish and screening for green fluorescence at 1 to 3 dpf.

**Generation of *valopa*<sup>-/-</sup> Fish using CRISPR/Cas9.** One-cell-stage zebrafish were co-injected with Cas9 mRNA and the sgRNA TCAGAGACACCGAAGT, designed to target the first exon of the *valopa* (NM\_131586) gene. One-day-old embryos were screened on the zBox for VALopA-induced photo-inhibition, and those with significantly diminished photo-inhibition responses were raised (*SI Appendix, Fig. S2A*). Potential founders were in-crossed and some progeny were found to have no photo-inhibition (*SI Appendix, Fig. S2B*). Genotyping of photo-insensitive F1 fish following behavioral testing revealed 19 different mutant alleles (*SI Appendix, Fig. S2C*). Genotyping was performed by amplifying a 222-bp section of the *valopa* gene using forward primer AGAACTCACCGTAATGCTGGT and reverse primer TGCATGAACCTTTTCACTGACC and sending purified PCR products for sequencing. Future generations of *valopa*<sup>-/-</sup> fish were in-crossed to obtain fish

that were homogeneous for the #6 mutant allele (*SI Appendix, Fig. S7C*) which were subsequently used for experiments.

**Preparation of Rat Primary Hippocampal Cultures.** Dissociated postnatal rat primary hippocampal cultures were dissected and cultured using a standard protocol (33) with a modification (the same media was used for plating and maintenance: Minimum Essential Media (Invitrogen) with 5% FBS (Hyclone), 2% B27 (Invitrogen), 1X Glutamax (Invitrogen), and 20 mM D-glucose, 1% serum extender). Neurons were plated onto poly-L-lysine coated 12-mm coverslips. Cultures were transfected with Lipofectamine 3000 according to the manufacturer's protocols at DIV6 and imaged DIV8. Then, 500 ng DNA/construct/coverslip was transfected. The mammalian transfection vector pcDNA3.1(+) was used for opsin transfection, and the pDEST47 transfection vector was used for Arl13b-GFP, as described below.

**Antibody Staining.** Embryos were fixed in 4% formaldehyde in PBS-T [16% Formaldehyde Solution (w/v), methanol Free, Thermo Scientific, 28906; PBS-T: 0.25% TX100 (Sigma) in PBS (Gibco), pH 7.2] for 3 h at R.T. with gentle shaking. Embryos were rinsed 3x in PBS-T and then permeabilized for 3 h with 3% TX100 in PBS at R.T. with gentle shaking. Blocking was done for 1 h in 5% NGS in PBS-T at R.T. with gentle shaking. Antibody staining was done overnight at 4 °C with gentle shaking. Antibodies used and dilutions are as follows: monoclonal anti-tubulin, acetylated antibody (mouse, Sigma Aldrich, T6793, clone 6-11B-1, 1:1,000 to 2,000); monoclonal anti-HA antibody (rabbit, Cell Signaling, C29F4, #3724, 1:500); goat anti-mouse IgG (H+L) Recombinant Secondary Antibody, Alexa Fluor 488 (Life Technologies A11001, 1:1,000); goat anti-Rabbit IgG (H+L) Superclonal Recombinant Secondary Antibody, Alexa Fluor 647 (Invitrogen, A27040, 1:1000). All antibodies were diluted into 5% NGS in PBS-T.

**Plasmid Construction and cRNA Synthesis.** VALopA cDNA was obtained and cloned as previously described (9). VALopB cDNA was a kind gift of Daisuke Kojima. The mnx1-3x125bp:Gal4-VP16 ("mnx:Gal4") plasmid with tol2 insertion sites was a kind gift from Juan Brusés. Rab23( constitutively active-Q68L) and Rab23(dominant negative-S23N) were ordered from IDT Technologies as a gBlock using the NCBI Reference Sequence: NM\_001020743 (danio rerio) with the added Q68L or S23N mutation. The Arl13b sequence was obtained from the plasmid pDEST47-Arl13b12-GFP, a gift from Tamara Caspary (Addgene #40872). To generate constructs for fish transgenic lines, VALopA-mKate2 and VALopB-mKate2 were cloned into the bidirectional UAS with Cerulean in the reverse direction as described in ref. 9 using the AclI and MluI sites to cut the backbone and followed by Gibson assembly. The long linker SRGTSGGSGSRGSGGSG bridges VALopB and mKate2. There is no linker between VALopA and mKate2. For transfection into mammalian cells, VALopA-mKate2 and VALopB-mKate2 (with linkers described above) were cloned into the pcDNA3.1(+) backbone BamHI and XhoI to cut the backbone followed by Gibson assembly. All VALop HA-tag containing constructs were cloned using Gibson assembly into the pCS2+ backbone using a linker SRGTSGGSG separating the upstream opsin and C-terminal HA tag, followed by LTGGGGS. For VALopB fusion proteins, the ciliary targeting protein was cloned downstream of the HA-LTGGGGS tag. Constructs with VALop-mKate2-P2A-Cerulean were cloned using Gibson assembly into the pCS2+ backbone using the long linker SRGTSGGSGSRGSGGSG separating the VALop and mKate2 sequences. The P2A sequence is flanked by linkers LTGE and TS on the 3' and 5' ends, respectively. Gibson reactions were performed with a homemade Gibson assembly mix (Phusion, T5-exonuclease, etc.). PCRs were performed using Phusion polymerase (NEB etc.) and 20- to 25-nt overlaps were used for all reactions. pGEMHE-GIRK1 (human, NM\_002239) and pGEMHE-GIRK2 (mouse, NM\_001025584) were used for oocyte experiments. Capped RNA was synthesized from constructs in the pCS2+ or pGEM backbone using the mMACHINE SP6 or T7, respectively, Transcription Kit according to the manufacturer's instructions. cRNA was stored at -20.

**In Situ Hybridization.** A fragment of VALopA (danio rerio, NM\_131586) was amplified by PCR using the One-Step RT-PCR kit (Invitrogen) with the following primers:

```
5'-TAATACGACTCACTATAGGGATGGAGGCGTCTCCGCGGCC-3'  
5'-CATGGGACACACTTGTCTCAGGTATGGGATGTGGCTG-3' (sense strand)  
5'-ATGGAGGCGTCTCCGCGGCCGTGAACGCGGTTCTCCCG-3'  
5'-TAATACGACTCACTATAGGGCATGGGACACACTTGTCTC-3'  
(anti-sense strand)
```

with the T7 promoter incorporated in the primers, and used to generate sense and antisense riboprobes with digoxigenin-labeled UTP (Roche, 11277073910). In situ hybridization was performed as described previously (34). For fluorescent in situ hybridization, anti-DIG POD (Roche 11633716001) was used at 1:400 dilution followed by tyramid amplification (Invitrogen, B40957). Briefly, embryos were fixed in 4% PFA and stored in methanol at -20 °C until use, then rehydrated step-wise to PBST (PBS with 0.1% tween 20). Embryos were permeabilized with proteinase k. Hybridization was carried overnight at 65 °C. Stained embryos were deyolked and mounted in 70% glycerol.

**Image Analysis.** To quantify cilium density, three 30- $\mu$ m-long sections of a dorsally mounted, MIP image of the spinal cord were delineated, and the number of cilia visible by eye in each section was counted. Cilia counts were averaged across the three regions. Motile and primary cilia within the spinal cord were counted together. The cumulative distribution functions for comparing B-Rab(CA)-mKate2 and B-Rab(DN)-mKate2 pixel intensities were generated using pixel intensities from the MIP of the stack of mKate2 images taken of the spinal cord. To quantify expression, average pixel intensity measurements were obtained from a single, mKate2 live image of the spinal cord by averaging 4 rectangular regions of the spinal cord, 2 regions on either side of the spinal canal, taken from the image plane in line with the spinal canal. Regions excluded the motile cilia in the spinal canal. Expression vs. PI data sets from Fig. 6 (VALopB vs B-Cil) and *SI Appendix, Fig. S10B* [B-Arl13b vs. B-Arl13b(PM)] were imaged separately during two different time periods with imaging parameters adjusted to roughly match expression levels.

**Alignment.** To obtain the approximate boundaries for intracellular and N-terminal domains of VALopA, the VALopA protein sequence was aligned to the rhodopsin crystal structure through two programs: UniProt and through the Modeller function in Chimera. VALopA (NP\_571661.1) was aligned to VALopB (NP\_001103750.1) in MATLAB using the *multialign* function with default properties. The borders of the N-terminus and intracellular domains used for domain swapping for VALopA and VALopB were liberally set to include neighboring AAs that differed in identity between VALopA and VALopB in order to capture any potential CTS's. For the VALopA full chimera ["A(Full Chimera)"], additional swapped AAs were added upstream of the original IL3 domain (denoted EXT in *SI Appendix, Fig. S3*) in order to ensure any potential CTS's in and around the IL3 would be tested.

**Oocyte Electrophysiological Recordings.** *Xenopus* oocytes were extracted and injected with cRNA as previously described (9). Briefly, following extraction of oocytes, the follicle cell layer was removed with sharp tweezers and cRNA was injected on the same day. GIRK1 and GIRK2 cRNA were combined in a 1:1 mass ratio (mix-GIRK) and then added to VALopX-HA or VALopX-mKate2-P2A-Cerulean cRNA in a 1:1 mixGIRK:VALopA (v/v) mix. Then, 50 nL of cRNA solution was injected into each oocyte with final concentrations of GIRK: ~1  $\mu$ g/ $\mu$ L and VALops: ~1.5  $\mu$ g/ $\mu$ L. cRNA was synthesized from pGEM (GIRKs) or pCS2+ (VALops) vectors as described above. Oocytes were incubated in ND96 (96 NaCl, 2 KCl, 1.8 CaCl<sub>2</sub>, 1 MgCl<sub>2</sub>, 50 mg/mL gentamicin, 2.5 Na<sup>+</sup>-pyruvate, and 5 HEPES, pH 7.6) at 16 °C for 2 d following injection with the buffer changed daily. Oocytes were incubated in 20  $\mu$ M 9-cis-retinal in ND96 for ~60 min and then washed before the start of recording. Recordings were performed on a Nikon Diaphot inverted microscope with a Dagan CA-1 amplifier (Dagan Corporation). A 150 W Xenon lamp for illumination was used with a 20x 0.75 NA fluorescence objective. Excitation light was passed through a HQ.TRITC excitation filter (535/50 nm, Chroma Technology) and ND4 filter. Whole-cell currents were measured using standard two-electrode voltage clamps procedures at RT(35). Recordings were performed in 96K solution (96 mM KCl, 2 mM NaCl, 1 mM CaCl<sub>2</sub>, 1 mM MgCl<sub>2</sub>, and 5 mM HEPES, pH 7.5). To extract kinetic parameters from the oocyte electrophysiological data, TAU-ON was calculated using a single exponential fit to the onset portion of the trace and T1/2-OFF was determined by assessing the timepoint at which the trace recovered to 1/2 of maximum amplitude.

**Data, Materials, and Software Availability.** All study data are included in the article and/or [supporting information](#). All data and analysis code have been deposited in Zenodo (36).

**ACKNOWLEDGMENTS.** We thank the members of the Isacoff lab for helpful discussions and support, especially, Krisha Aghi for advice on the statistical analysis in Fig. 6, Prashant Donthamsetti for assistance on the VALopA/ rhodopsin alignment, Adam Hoagland for technical assistance with the zBox and scripting, Yael Isacoff for help with the oocyte experiments, and Victoria

Chou for many key pieces of advice. We thank Juan Brusés for cDNA encoding mnx1-3x125bp:Gal4-VP16 and Daisuke Kojima for cDNA encoding VALopB. Lattice light sheet imaging experiments were conducted at the Janelia Research Campus, and we thank Eric Betzig for his supervision and support. Confocal imaging experiments were conducted at the University of California Berkeley Cancer Research Laboratory Molecular Imaging Center, supported by the University of California Berkeley Helen Wills Neuroscience Institute and the NIH (RRID:SCR\_017852), and we thank Holly Aaron and Feather Ives for their microscopy advice. Additional thanks to the Zebrafish Facility at University of

California Berkeley. This work was supported by a NIH postdoctoral fellowship (1F32NS100387; A.M.W.) and grants (R01NS119826 and R01EY028240-01A1; E.Y.I., and NIH GM79465; T.X. and C.J.C.).

Author affiliations: <sup>a</sup>Department of Molecular and Cell Biology, University of California, Berkeley, CA 94720; <sup>b</sup>Department of Chemistry, University of California, Berkeley, CA 94720; <sup>c</sup>HHMI, Janelia Research Campus, Ashburn, VA 20147; <sup>d</sup>Helen Wills Neuroscience Institute, University of California, Berkeley, CA 94720; <sup>e</sup>Molecular Biophysics and Integrated BioImaging Division, Lawrence Berkeley National Laboratory, Berkeley, CA 94720; and <sup>f</sup>Weill Neurohub, University of California, Berkeley, CA 94720

1. J. F. Reiter, M. R. Leroux, Genes and molecular pathways underpinning ciliopathies. *Nat. Rev. Mol. Cell Biol.* **18**, 533–547 (2017), 10.1038/nrm.2017.60.
2. M. V. Nachury, D. U. Mick, Establishing and regulating the composition of cilia for signal transduction. *Nat. Rev. Mol. Cell Biol.* **20**, 389–405 (2019), 10.1038/s41580-019-0116-4.
3. D. Wachten, D. U. Mick, Signal transduction in primary cilia—analyzing and manipulating GPCR and second messenger signaling. *Pharmacol. Ther.* **224**, 107836 (2021), 10.1016/j.pharmthera.2021.107836.
4. S. M. Park, H. J. Jang, J. H. Lee, Roles of primary cilia in the developing brain. *Front. Cell Neurosci.* **13**, 1–10 (2019), 10.3389/fncel.2019.00218.
5. M. E. Truong *et al.*, Vertebrate cells differentially interpret ciliary and extraciliary cAMP. *Cell* **184**, 2911–2926.e18 (2021), 10.1016/j.cell.2021.04.002.
6. J. E. Siljee *et al.*, Subcellular localization of MC4R with ADCY3 at neuronal primary cilia underlies a common pathway for genetic predisposition to obesity. *Nat. Genet.* **50**, 180–185 (2018), 10.1038/s41588-017-0020-9.
7. E. B. Einstein *et al.*, Somatostatin signaling in neuronal cilia is critical for object recognition memory. *J. Neurosci.* **30**, 4306–4314 (2010), 10.1523/JNEUROSCI.5295-09.2010.
8. S. H. Sheu *et al.*, A serotonergic axon-cilium synapse drives nuclear signaling to alter chromatin accessibility. *Cell* **185**, 3390–3407.e18 (2022), 10.1016/j.cell.2022.07.026.
9. D. Friedmann, A. Hoagland, S. Berlin, E. Y. Isacoff, A spinal opsin controls early neural activity and drives a behavioral light response. *Curr. Biol.* **25**, 69–74 (2015), 10.1016/j.cub.2014.10.055.
10. D. Kojima, H. Mano, Y. Fukada, Vertebrate ancient-long opsin: A green-sensitive photoreceptive molecule present in zebrafish deep brain and retinal horizontal cells. *J. Neurosci.* **20**, 2845–2851 (2000).
11. D. Kojima, M. Torii, Y. Fukada, J. E. Dowling, Differential expression of duplicated VAL-opsin genes in the developing zebrafish. *J. Neurochem.* **104**, 1364–1371 (2008), 10.1111/j.1471-4159.2007.05093.x.
12. E. Warp *et al.*, Emergence of patterned activity in the developing zebrafish spinal cord. *Curr. Biol.* **22**, 93–102 (2012), 10.1016/j.cub.2011.12.002.
13. L. Saint-Amant, P. Drapeau, Synchronization of an embryonic network of identified spinal interneurons solely by electrical coupling. *Neuron* **31**, 1035–1046 (2001), 10.1016/S0896-6273(01)00416-0.
14. H. Baier, E. K. Scott, Genetic and optical targeting of neural circuits and behavior—zebrafish in the spotlight. *Curr. Opin. Neurobiol.* **19**, 553–560 (2009), 10.1016/j.conb.2009.08.001.
15. C. Wyart *et al.*, Optogenetic dissection of a behavioural module in the vertebrate spinal cord. *Nature* **461**, 407–410 (2009), 10.1038/nature08323.
16. N. Dale, A. Roberts, O. P. Ottersen, J. Storm-Mathisen, The morphology and distribution of “Kolmer-Agduhr cells”, a class of cerebrospinal-fluid-contacting neurons revealed in the frog embryo spinal cord by GABA immunocytochemistry. *Proc. R. Soc. Lond. B Biol. Sci.* **232**, 193–203 (1987), 10.1098/rspb.1987.0068.
17. U. L. Böhm *et al.*, CSF-contacting neurons regulate locomotion by relaying mechanical stimuli to spinal circuits. *Nat. Commun.* **7**, 10866 (2016), 10.1038/ncomms10866.
18. T. L. Liu *et al.*, Observing the cell in its native state: Imaging subcellular dynamics in multicellular organisms. *Science* **360**, eaq1392 (2018), 10.1126/science.aq1392.
19. T. Caspary, C. E. Larkins, K. V. Anderson, The graded response to sonic hedgehog depends on cilia architecture. *Dev. Cell* **12**, 767–778 (2007), 10.1016/j.devcel.2007.03.004.
20. B. U. Klink *et al.*, A recombinant BBSome core complex and how it interacts with ciliary cargo. *Elife* **6**, 1–21 (2017), 10.7554/eLife.27434.
21. N. F. Berbari *et al.*, Identification of ciliary localization sequences within the third intracellular loop of G protein-coupled receptors. *Mol. Biol. Cell* **19**, 1540–1547 (2008), 10.1091/mbc.E07.
22. A. Leaf, M. Von Zastrow, Dopamine receptors reveal an essential role of IFT-B, KIF17, and Rab23 in delivering specific receptors to primary cilia. *Elife* **4**, 1–23 (2015), 10.7554/eLife.06996.
23. C. Pantoja *et al.*, Measuring behavioral individuality in the acoustic startle behavior in zebrafish. *Bio Protoc.* **7**, e2200 (2017), 10.21769/BioProtoc.2200.
24. D. Kokel *et al.*, Identification of nonvisual photomotor response cells in the vertebrate hindbrain. *J. Neurosci.* **33**, 3834–3843 (2013), 10.1523/JNEUROSCI.3689-12.2013.
25. A. L. Duncan, W. Song, M. S. P. Sansom, Lipid-dependent regulation of ion channels and g protein-coupled receptors: Insights from structures and simulations. *Annu. Rev. Pharmacol. Toxicol.* **60**, 31–50 (2020), 10.1146/annurev-pharmtox-010919-023411.
26. L. De Vries *et al.*, The regulator of G protein regulation of G protein-coupled receptor signaling. *Annu. Rev. Pharmacol. Toxicol.* **40**, 235–271 (2000).
27. V. V. Gurevich, E. V. Gurevich, GPCR signaling regulation: The role of GRKs and arrestins. *Front. Pharmacol.* **10**, 1–11 (2019), 10.3389/fphar.2019.00125.
28. S. C. Phua, Y. Nihongaki, T. Inoue, Autonomy declared by primary cilia through compartmentalization of membrane phosphoinositides. *Curr. Opin. Cell Biol.* **50**, 72–78 (2018), 10.1016/j.cub.2018.01.008.
29. M. Kinnebrew *et al.*, Cholesterol accessibility at the ciliary membrane controls hedgehog signaling. *Elife* **8**, 1–28 (2019), 10.7554/eLife.50051.
30. M. Jafurulla, G. Aditya Kumar, B. D. Rao, A. Chattopadhyay, A critical analysis of molecular mechanisms underlying membrane cholesterol sensitivity of GPCRs. *Adv. Exp. Med. Biol.* **1115**, 21–52 (2019).
31. J. A. Green *et al.*, Recruitment of  $\beta$ -arrestin into neuronal cilia modulates somatostatin receptor subtype 3 ciliary localization. *Mol. Cell Biol.* **36**, 223–235 (2015), 10.1128/MCB.00765-15.
32. T. A. Zelenchuk, J. L. Brusés, In vivo labeling of zebrafish motor neurons using an mnx1 enhancer and Gal4/UAS. *Genesis* **49**, 546–554 (2011), 10.1002/dvg.20766.
33. G. M. J. Beaudoin *et al.*, Culturing pyramidal neurons from the early postnatal mouse hippocampus and cortex. *Nat. Protoc.* **7**, 1741–1754 (2012), 10.1038/nprot.2012.099.
34. T. Xiao *et al.*, Copper regulates rest-activity cycles through the locus coeruleus-norepinephrine system. *Nat. Chem. Biol.* **14**, 655–663 (2018), 10.1038/s41589-018-0062-z.
35. N. Dascal, Voltage clamp recordings from Xenopus oocytes. *Curr. Protoc. Neurosci.* **10**, Chapter 6, Unit 6.12 (2000), 10.1002/0471142301.ns0612s10.
36. A. M. Winans *et al.*, Ciliary localization of a light-activated neuronal GPCR shapes behavior. Zenodo. <https://doi.org/10.5281/zenodo.8411217>. Deposited 5 October 2023.